Experimental research on multichannel discharge circuit and multi-electrode plasma synthetic jet actuator

Zhibo ZHANG[1], Yun WU[1,2*], Zhengzhong SUN[3],Huimin SONG[1],
Min JIA[1], Haohua ZONG[2], Yinghong LI[1]

1 Science and Technology on Plasma Dynamics Laboratory, Air Force Engineering University, Xi'an, 710038, People's Republic of China

2 Science and Technology on Plasma Dynamics Laboratory, Xi'an Jiaotong University, Xi'an, 710049, People's Republic of China

3 Department of Mechanical Engineering and Aeronautics, City University London, London, United Kingdom

Abstract: To solve the low efficiency of plasma synthetic jet actuator (PSJA), a multichannel discharge technique based on the concept of voltage relay is put forward and a new multi-electrode plasma synthetic jet actuator (ME-PSJA) is designed. Experiment shows the multichannel discharge technique can enlarge the discharge channel distance by multiplying the discharge channel number without increasing the input voltage. With a 1 nF discharge capacitor, the discharge efficiency of three channels discharge increases 135% compared with standard one channel discharge. When the discharge capacitor increases to 0.3 μF, a four discharge channels still improves the discharge efficiency 119 % as well. Schlieren flow visualization confirms that ME-PSJA also outperforms the 2-electrode PSJA in terms of jet velocity and duration time, both are increased by about 50%.

Keywords: flow control; plasma actuator; plasma synthetic jet; discharge efficiency

0 Introduction

There has always been continuous effort in the development of active flow control so as to improve the performance of aerodynamic applications. Different from the passive control device, the active control has the benefit of being adaptive to the flow condition, and can be switched off when control is not needed. The plasma synthetic jet actuator (PSJA) is one novel active flow control technique, and it is believed to have promising capability in the transonic and supersonic regime. Originally proposed in 2003 by the Johns Hopkins University[1]， applications of PSJA can be seen in shock wave boundary layer interaction (SWBLI)[2,3] and shock wave manipulation[4,5].

The PSJA has been under continuous development. The evolution of the PSJA technique is summarized in Figure 1 graphically. In general, there are two generations of PSJA and they are distinguished through the number of electrodes. The first generation features two electrodes, namely dual-electrode PSJA (DE-PSJA). The early research in the Johns Hopkins University showed the DE-PSJA can produce high speed jet and has potential application for high-speed flows [6-13], which supplements DBD type actuator's low-speed applications. On the other hand, the drawback of PSJA's low efficiency has been identified, which hinders its practical usage. Various researches pointed out its efficiency is less than 30% [14-17], sometimes it is even less than 1% [18,19]. It is eventually found that the efficiency is affected by the electrode gap distance. Our experiment also showed that a PSJA with 3 mm electrode distance can generate strong jet, while that with 0.5 mm electrode distance cannot generate jet[20]. The second generation PSJA emerges with longer electrode gap by adding a third electrode, namely the trigger electrode. The second generation also has the name three-electrode PSJA (TE-PSJA)[15]. With the help of electronic element, such as magnetic switch and diode, the anode and trigger electrode can be hold together[19-21]. In this condition, the TE-PSJA can be improved to two-electrode PSJA. The TE-PSJA has already been used by several researchers[22-26]. However, as

the electrode gap of the TE-PSJA is determined by the voltage of trigger power supply, there is an upper limit for the gap distance. If the gap exceeds the critical distance, no discharge will take place. As a result, the further improvement is restricted by the critical gap distance and breakthrough in technology is required.

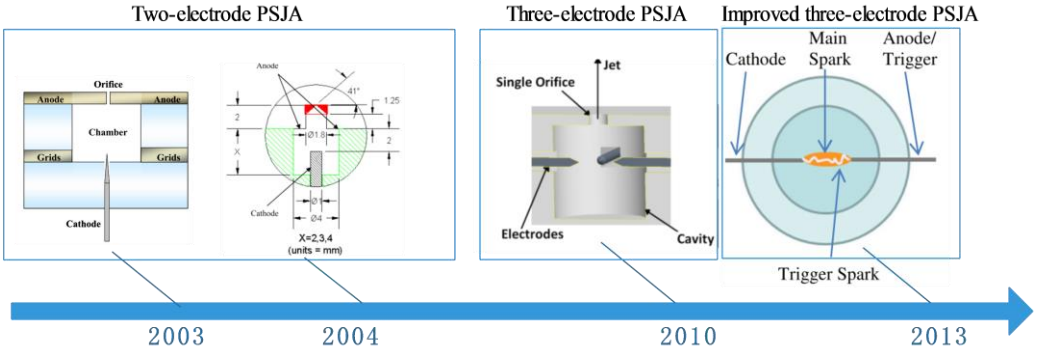

Figure 1. The development of the PSJA

In the present work, a new discharge concept of voltage relay is developed. This concept allows to enlarge the gap distance without any increase in input voltage. Using the voltage relay concept, a new discharge circuit and a new PSJA, namely the multi-electrode PSJA (ME-PSJA), are proposed. In order to validate the new ME-PSJA, its aerodynamics performance is validated experimentally through schlieren.

1 A new concept to enlarge the distance of discharge channel

The discharge circuit of the first generation DE-PSJA is simplified in Figure 2 (a). The discharge current of the DE-PSJA is a sinusoidal oscillating signal and the amplitude follows the damped exponential law, as shown in Figure 2(a). When the voltage begins to decrease and the current begins to increase heavily, it is the time that the process of breakdown has terminated and the process of discharge has started. Therefore, only a little fraction of the pulsed energy is used to trigger the discharge and build the discharge channel. A large portion of the energy is consumed in the discharge process. The resistance in the plasma region is subject to dramatic change as shown in Figure 2(c). The change of plasma resistance can be divided into two processes, namely the breakdown process and discharge process. As long as the voltage across the discharge electrodes is higher than the corresponding breakdown voltage, the breakdown process will happen. Therefore, if the voltage can remain unchanged and can be relayed to the next discharge electrodes, the discharge channel would be increased. In this way, the total distance of the channel can be enlarged.

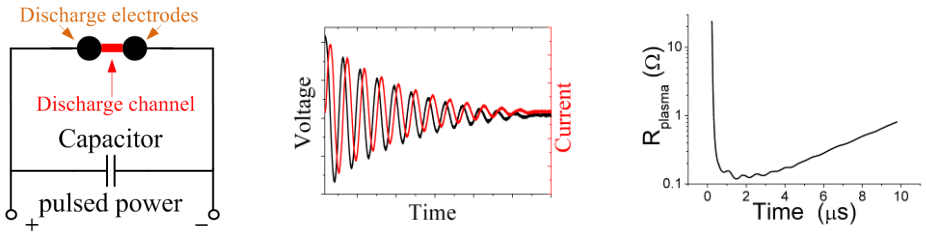

Figure 2. Characteristics of discharge circuit of two-electrode PSJA: (a) simplified circuit (b) evolution of discharge voltage and current (c) evolution plasma resistance

Due to the negative resistance characteristics of the discharge channel, when the breakdown of the discharge gap happens, the plasma resistance decrease quickly. As a result, the energy stored in the capacitor is consumed by discharge quickly. Therefore, a larger impedance of the discharge circuit is preferred to reduce the discharge rate. But large impedance may result in a small current, which

eventually makes the discharge channel to quench. Taking these factors into consideration, a special discharge circuit is designed.

A baseline test circuit is thus proposed to provide the voltage relay with appropriate circuit impedance as shown in Figure 3 (a). The discharge voltage and current are measured with a high voltage probe (Tektronix P6015A) and a current probe (Tektronix TCP312), respectively. The measurement positions are labelled in figure 3(a). The voltage and current are recorded by an oscilloscope (Tektronix DPO4140). The waveforms are shown in Figure 3 (b), which is different from the conventional circuit as previously shown in figure 2(b). As soon as the breakdown of the electrode gap happens, the voltage at point 2 increases rapidly and reaches its peak value in 25 ns. The current quickly increases to 8 A in less than 20 ns and then decreases to 0 A. Because of the large difference between the capacitor C and C_1, and the low energy required to build the discharge channel, the voltage at position 1 has little change during breakdown. Meanwhile, the voltage at position 2 increases to a high value and can be used to build the next discharge channel.

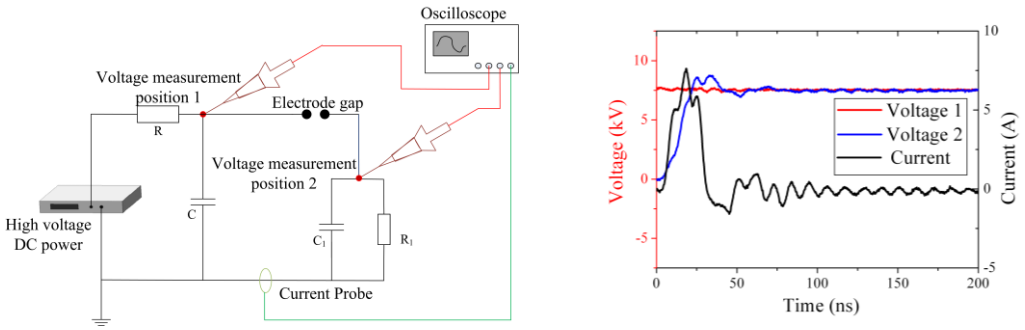

(a) The experimental system (b) The typical current and voltage history

Figure 3. The special discharge circuit experiment

Following the baseline test circuit in Figure 3, a special discharge component can be established, as shown in Figure 4(a). In this circuit, the capacitor and resistor has the name of relay capacitor and relay resistor, respectively. The capacitance of relay capacitor is larger than the equivalent capacitance of electrode gap. It is known that the capacitor impedance goes down as capacitance goes up. Hence, before the breakdown of the electrode gap, the voltage across the electrode gap is the same as the input voltage, but the output voltage is zero. As soon as the breakdown happens, the impedance of the electrode gap decreases rapidly, and the relay capacitor is charged, raising the output voltage, which can be used to drive the next discharge element. The relay resistor is used to absorb the residual energy in the relay capacitor, as the discharge in the relay capacitor, in practice, is usually incomplete. Because the gap needs to be ignited in a repetition mode, the residual energy in the relay capacitor has to be released. Otherwise, the breakdown voltage will not be reached across the gap.

Taking these factors into consideration, the resistance of relay resistance should meet the condition, as shown in Eq.(1). In this relationship, t_1 represents the time needed to build the complete discharge channel in the multichannel discharge circuit, which is in order of microsecond. t_2 indicates the discharge time interval, which is determined from the repetition rate f, $t_2=1/f$.

$$t_1 << 5R_{relay}C_{relay} << t_2 \quad (1)$$

Using this discharge component, a new circuit containing multichannel discharge can be built, as shown in Figure 4(b). This discharge circuit operates in a relay style. After the breakdown of electrode gap 1, the voltage across the electrode gap 2 increases, leading to the breakdown in electrode gap 2. The breakdown in the rest electrode gaps takes place in a replay manner. As a result, this 'relay' discharge circuit increases the discharge gap through increasing the number of discharge channel.

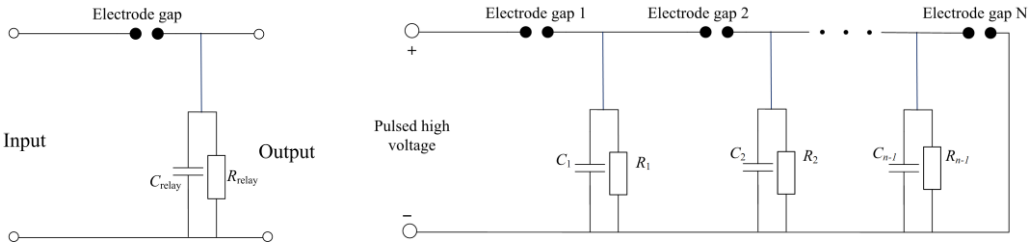

(a) the discharge component (b) the complete discharge circuit

Figure 4. the schematic diagram of the relay multichannel discharge circuit

2 Experiment on the multichannel discharge circuit

2.1 Experimental circuit

A prototype circuit containing four discharge channels is built for validation purpose, as shown in Figure 5. A high voltage DC power is used to charge the main discharge capacitor C (1 nF) through a 10 MΩ current-limiting resistor R_{lim}. The relay capacitance of C_1, C_2, and C_3 is 100 pF, while the resistance of R_1, R_2, and R_3 is 1 MΩ. This prototype circuit also allows to change the number of channels through reducing the electrode gap down to zero. For instance, a three-channel discharge circuit is realized by setting the distance of electrode gap 4 to 0. The measurement system is the same as that used in test in the previous section. In the following, V_1, V_2 and V_3 are used to represent the voltage measured at point 1, 2 and 3, respectively.

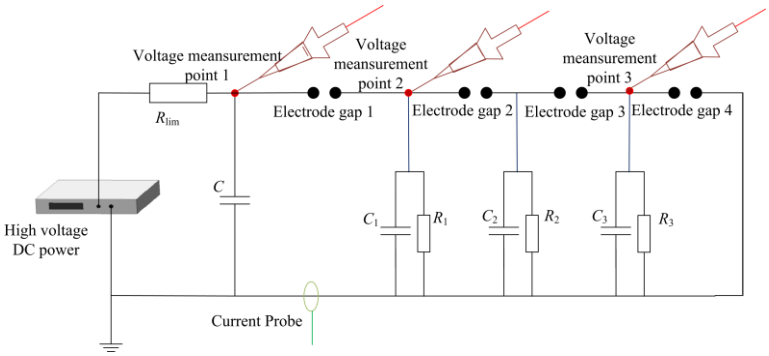

Figure 5. the schematic diagram of the prototype relay circuit

2.2 Results and discussion

2.2.1 The electric characteristics

A three-channel discharge is first conducted to reveal the electric characteristics. The length of electrode gap 1, 2, 3 and 4 are thus set to 2 mm, 2 mm, 2 mm and 0 mm, respectively. The measured discharge voltage (V_1, V_2) and current waveforms are shown in Figure 6. The breakdown of the electrode gap 1 leads its impedance to decrease. The capacitor C_1 is then charged. As a result, the voltage V_2 increases to 9.4 kV in less than 30 ns, giving rise to the breakdown in gap 2. Because of the large capacitance of main discharge capacitor C, V_2 only decreases slightly before the breakdown of gap 3. The next capacitor C_2 is further charged following the breakdown of electrode gap 2, and the voltage across C_2 increases. Similarly, when the voltage across gap 3 reaches to its breakdown voltage, the breakdown in gap 3 happens, and a complete discharge channel is built. At this moment, the current increases to about 100 A quickly.

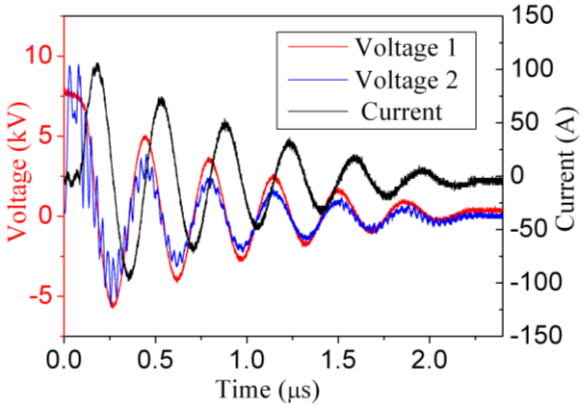

Figure 6. The multichannel discharge voltage and current waveforms

In conclusion, the breakdown of electrode gaps happens sequentially. The capacitor and resistor connected to the electrode gap are critical. They must secure the sequential breakdown for the gaps. Before the breakdown, the gap can be seen as an open switch. It acts as a small resistor after breakdown takes place. Since the breakdown changes sequentially, the circuit also changes. The equivalent circuits after each breakdown is shown in Figure 7.

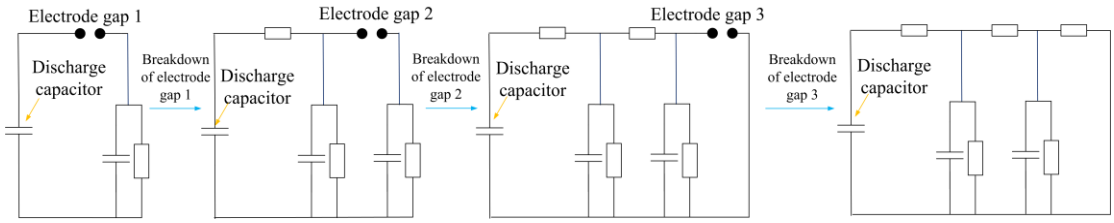

Figure 7. Equivalent circuits after three sequential discharges

The input power voltage and the peak current with different channel numbers and different distances of electrode gap are shown in Figure 8 (a) and Figure 8 (b), respectively. Note that the input power voltage is the voltage at measurement point 1 before the breakdown of the electrode gap 1 for each test. The horizontal axis is the length of a single discharge channel.

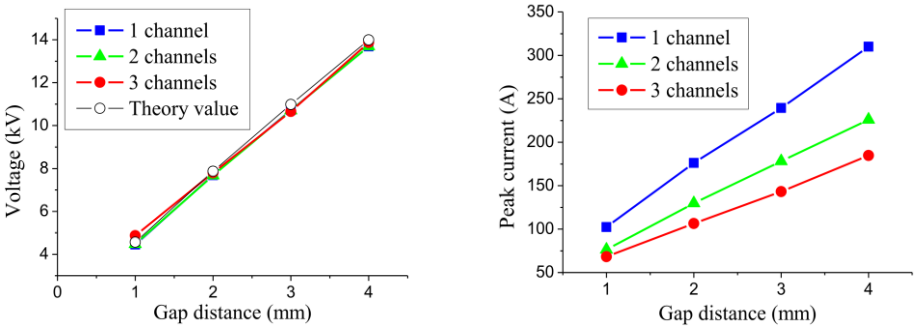

(a) The input power voltage (b) The peak current

Figure 8. Effect of the number of discharge channel and gap distance on breakdown voltage and peak current

The input power voltage can be theoretically predicted through the following relation[27]:

$$U_{\text{breakdown}} = 2.436pd + 6.72\sqrt{0.1pd} \quad \text{(kV)} \qquad (2)$$

where p is the pressure (unit: bar), d is the distance between the electrode couple (unit: millimeter). The breakdown voltage estimated theoretically using Eq. (2) is also included in Figure 8 (a). It can be found that the experimental data and theoretical data have a good agreement. The input voltages almost grow

linearly with the increase of gap distance. The number of channels seems to have trivial effect on the breakdown voltage, as little variation can be observed by adding more channels. On the other hand, increasing the number of discharge channel essentially results in a larger total discharge length, giving rise to a larger plasma resistance. As a result, the peak current decreases. The influence of channel number on the peak current is presented in Figure 8 (b).

Different from the conventional single channel discharge, there is an obvious breakdown discharge process in the new circuit. The current and voltage at measurement position 1 with 2 mm gap distance are shown in Figure 9 (a) and Figure 9 (b), respectively. It is rather apparent that the voltage drop for two-channel discharge and three-channel discharge is less steep at the initial phase. In the meantime, there is a delay in current increase for the multi-channel discharge. In the present test, the current increase for 2-channel discharge and 3-channel discharge are at 53 ns and 108 ns, respectively, which are the amount of time needed to build the complete discharge channel. Therefore, longer time is needed to trigger the discharge for a greater number of channels.

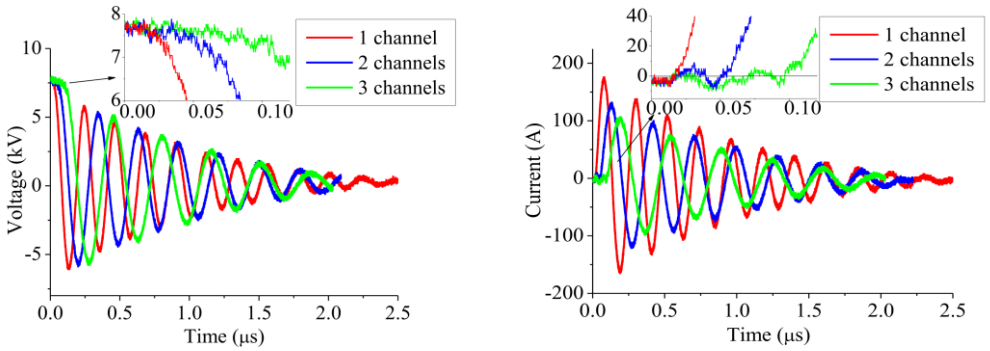

(a) The voltage (b) The current

Figure 9. Voltage and current waveforms for single and multi-channel discharges

2.2.2 The influence of the discharge capacitor on the multichannel discharge circuit

The circuit is further made into a four-channel discharge circuit by increasing the fourth gap distance from 0 to 3 mm. The discharge capacitor is changed from 1 nF to 3.2 nF to study the effect of discharge capacitor. The increase of the capacitor is made through parallel connecting another capacitor of 2.2nF.

In case of smaller capacitor (C=1 nF), breakdown only happens in the first three gaps except gap 4. This condition is named the incomplete discharge. As the relay capacitance is larger (1 MΩ), the current flowing the electrode gap is very low, depositing small energy. Based on arc energy balance theory, the discharge channel in gap 1, gap 2 and gap 3 would terminate quickly, and the energy stored in the discharge capacitor cannot be released completely. The waveforms of voltages at position 1 and 3 and current are shown in Figure 10 (a). Because part of the input energy is consumed in the breakdown discharge process and to charge the relay capacitor, the voltage at position 1 decreases from 13.8 kV to nearly 10.5 kV after 200 ns, which is highlighted by the pink arrow. This voltage drop together with the voltage waveform shown in Figure 3 (b) indicate that the energy stored in the discharge capacitor isn't enough to provide sufficient voltage.

In case of larger capacitor (C=3.2 nF), breakdown happens in all four electrode gaps, namely the complete discharge. As a result, the circuit impedance decreases quickly, and the current increases to about 300 A. The energy stored in the discharge capacitor can be released in the discharge process, and the voltage across capacitor eventually becomes zero. The discharge voltage and current waveforms are represented in Figure 10 (b). The breakdown of the fourth channel, namely the decrease of V_3, happens

at around 270 ns, when V_1 is about 12.2 kV. It should be noted that there is no significant voltage drop in V_1, despite the small oscillation. So far it reveals that the discharge capacitance is critical in the breakdown process. It should be large enough to secure the breakdown of the discharge channel.

So far, it can be understood that a larger discharge capacitor is necessary when the discharge channel number increases. As discussed above, the relay capacitor is charged with the breakdown of electrode gap. As a result, with the increase of number of electrode gap, more energy is needed. But the maximum voltage across the discharge capacitor is determined by the corresponding breakdown voltage of the first electrode gap. As a result, the more the electrode gap is, the larger the capacitance of the discharge capacitor needs to be.

In addition, the distance of total discharge channel increases with growth of discharge channel number naturally. This means that the distance of total discharge channel increases with the raise of the discharge capacitor. In the previous study, the only way to increase the discharge channel distance is to increase the input voltage. The present conclusion is potential in solving the problem that the efficiency of the PSJA decreases with the increase of capacitance[17].

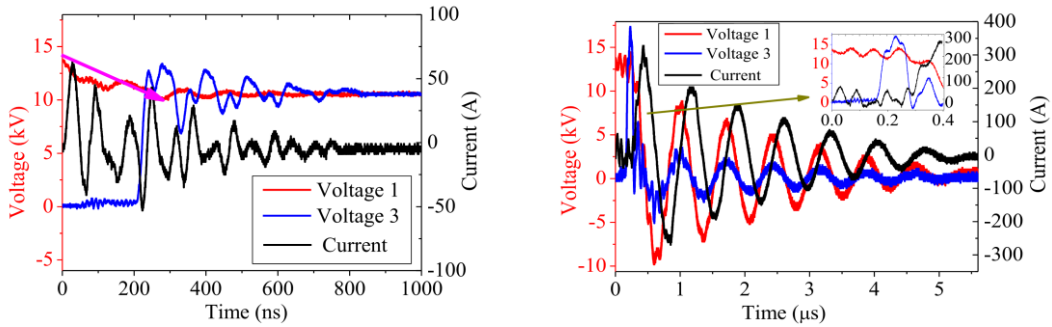

(a) The incomplete discharge (b) The complete discharge

Figure 10. The voltage and current waveforms for 4 discharge channels

2.2.3 The discharge efficiency

The discharge characteristic of the multi-channel circuit is similar as the typical discharge in RLC circuit. The plasma region can be modeled as a constant resistor in a simplified calculation[28]. The discharge current can be obtained as following:

$$i_d(t) = A \cdot e^{-at} \cdot \sin(\omega t) \quad (3)$$

where A, α, and ω are determined by the circuit resistor, inductor, capacitor, and the initial voltage. In the present circuit, the capacitor is constant. The initial voltage is obtained from measurement. The resistor can be found through fitting the current returned by Eq.(3) with the measured current waveform, as shown in Figure 11.

Using this method, the plasma resistances for different channels are compared in Figure 12. The increase of plasma resistance is non-linear when the number of channel increases. When one channel is used, the plasma resistance is 1.51 Ω. Increasing the number of channels to two, the plasma resistance becomes 3.16 Ω. A three channel circuit results in a plasma resistance of 5.3 Ω. Moreover, with the increase of the discharge channel number, the discharge current decreases. Based on the arc-resistance models[29], the resistance of spark channel is negatively related to the discharge current. As a result, the resistance of a single channel with the same length also increases.

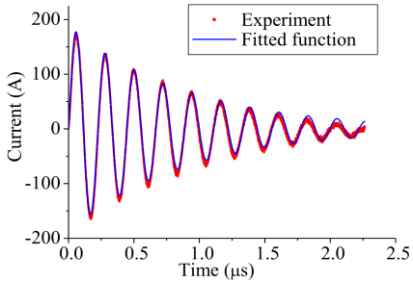

Figure 11. The fitting curve of the discharge current

Knowing the plasma resistance, the total discharge efficiency is calculated as the ratio of plasma resistance and the circuit total resistance, as shown in Eq.(4).

$$\eta = \frac{R_{\text{plasma}}}{R_{\text{total}}} \qquad (4)$$

As shown in Figure 12, the one-channel circuit thus has efficiency of 54%. It is improved by increasing the number of channels. The plasma resistance in the present three-channel circuit is 135% of that of a one-channel circuit. However, the efficiency improvement is only 48%. The slower improvement in efficiency can be attributed to circuit resistance, which is critical in determining discharge efficiency. The circuit resistance includes the wire resistance and the equivalent series resistance of the discharge capacitor. The effect of circuit resistance is also simulated and the result is shown in Figure 13. The number of discharge channels is simplified represented by the increasing magnitude of plasma resistance. All the five curves, each of which has constant circuit resistance, exhibit the same trend. A rapid growth in efficiency happens when plasma resistance is initially increased, but the growth becomes slower when plasma resistance is further increased. This effect is delayed when a larger circuit resistance is present. Therefore, this multichannel discharge circuit can play an import role in practical application, where the $R_{\text{wire,c}}$ is relatively large.

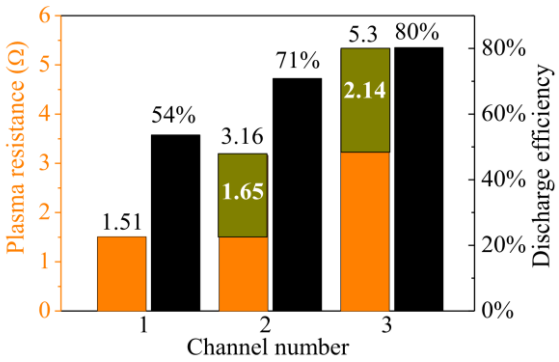

Figure 12. The plasma resistance and discharge efficiency versus the discharge channel number

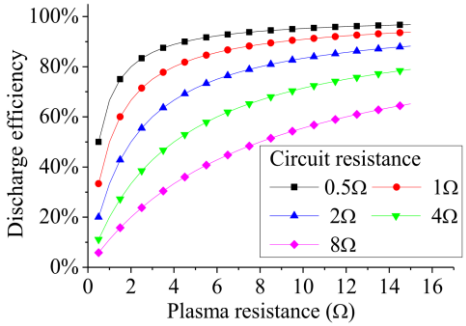

Figure 13. Influence of circuit resistance on discharge efficiency

3 Experiment on the ME-PSJA

3.1 The Actuator and Experimental Setup

A ME-PSJA using the multi-channel discharge circuit is further test. The present actuator features conventional cavity-cap structure, and it is shown in Figure 14. The ceramic cavity has height and the inner diameter of 15 mm. There are five tungsten electrodes in the cavity and the distance between the neighboring ones is 3 mm. The cap is made of copper. An orifice is equipped in the center with diameter of 3 mm. The power supply system uses the multichannel discharge circuit, which is similar as shown in Figure 5. In order to ensure the strength of the jet, a large discharge capacitor of 0.3 μF is chosen. This circuit also allows to change the number of discharge channel through different wire connections.

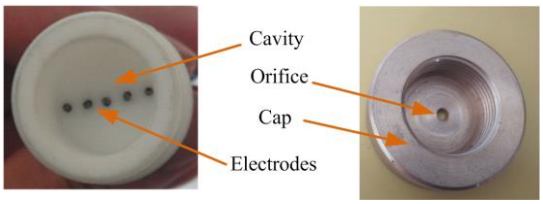

(a) The components

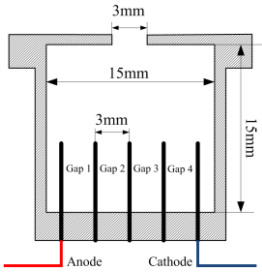

(b) The diagram

Figure 14. The multi-electrode PSJ actuator

A Z-type schlieren system is used for visualizing the generated jet flow. The illumination is provided by a Xenon lamp. A Phantom V2511 high-speed camera is used to record the images. It operates at a frame rate of 170,157 fps, the exposure time is chosen at 0.92 μs.

3.2 Results and discussion

3.2.1 The discharge characteristics

The discharge current is shown in Figure 15. With the increase of the discharge channel number, the current attenuation increases. This suggests that the total resistance in the discharge circuit increases. Taking the constant wire resistance and equivalent series capacitor resistance into consideration, it is believed that the increase of resistance is caused by the increase of discharge channel number.

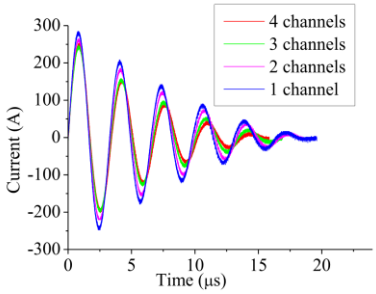

Figure 15. The discharge current waveform

The plasma resistance can be calculated from the recorded discharge voltage and current, and the discharge efficiency can be further calculated through equation (3). The results are shown in Figure 16. Both quantities grow following the increase of discharge channel number. As revealed above, the growth of discharge efficiency lags behind the increase of plasma resistance. The four-channel discharge has plasma resistance about four times of that in single-channel, but its discharge efficiency is only doubled.

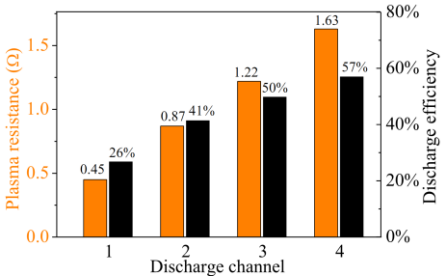

Figure 16. The plasma resistance and discharge efficiency for discharge with different channel number

The discharge process is recorded through a Nikon D7000 camera, equipped with 34 mm focal length lens. The lens aperture is set $f_{\#}$/6.3, shutter speed 1/320 s, ISO 100. The recorded discharge images are shown in Figure 17Figure 16. Apparently, the more channels are used, the stronger light intensity is produced by the spark light, suggesting that more energy is deposited.

Figure 17. The discharge images for actuator with different number of discharge channels (the discharge channel increases from one to four from left to right)

3.2.2 The jet characteristics

The high-speed schlieren system allows of time-resolved imaging of the jet flow. The growth of the jet generated by the actuator with different channels is shown through five snapshots in Figure 18. A rectangle is used to highlight the turbulent jet. Its height and width in each snapshot are determined by the jet of the four-channel actuator. Overlapping this rectangle in the jet of other actuators allows the comparison of the jet size. It can be found that the jet from the single-channel actuator is significantly smaller than those from multi-channel actuators, suggesting that the jet velocity is also much smaller. Although there is no big difference in jet size at 147 us for the multi-channel actuators, following their development, the more channels the actuator has, a larger jet is produced. Again, it infers that the four-channel actuator provides the strongest jet.

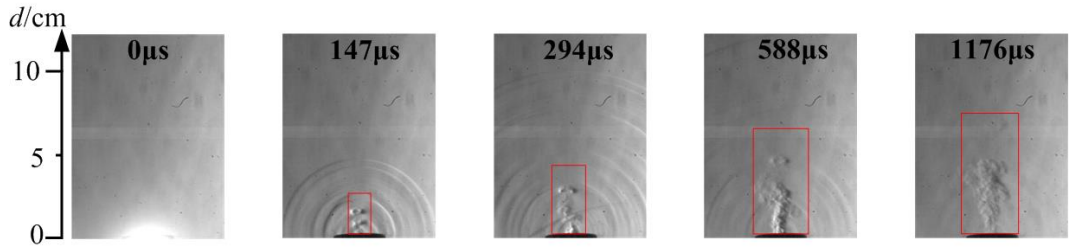

(a) One discharge channel

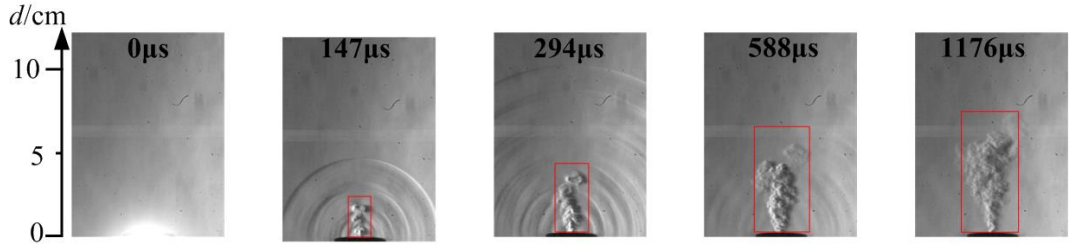

(b) Two discharge channels

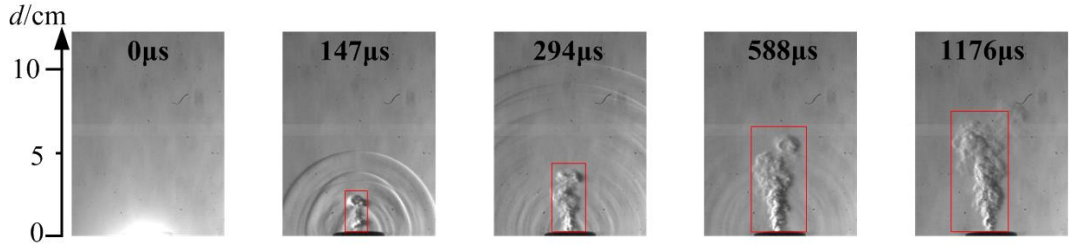

(c) Three discharge channels

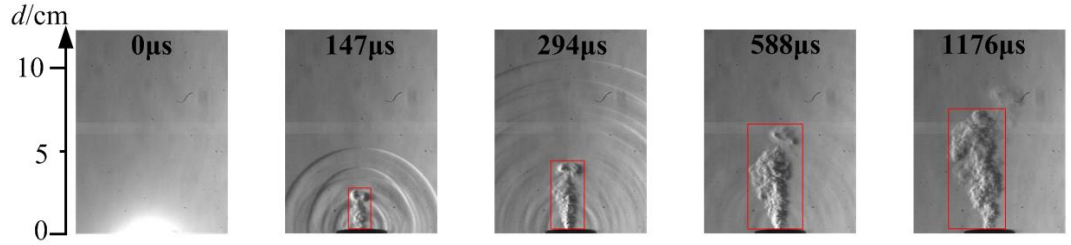

(d) Four discharge channels

Figure 18. Schlieren images of the jet at given time steps with different discharge channel number

The jet velocity is further estimated through the motion of turbulent jet front, which can be identified in the schlieren images. The jet velocity at 147 μs for all the four actuators is compared in Figure 19. The four-channel actuator has the largest jet velocity of 180 m/s, which is 1.5 time of that of single channel actuator. Although the jet velocity increases by increasing the number of channels, the increase becomes smaller, which means jet velocity is going to be only slightly increased when more channels are used.

Based on the method described in [21], the jet duration time is also estimated through schlieren recordings. The jet lasts longer when the actuator has more channels, as shown in Figure 19. For example, the jet generated by four-channel actuator lasts 50% longer than that of a single-channel actuator. Again the increase of jet duration time slows down when additional channels are further added. In summary, the multi-channel actuator generally generates stronger jet with longer duration time. However, the performance improvement slows down gradually when more channels are used.

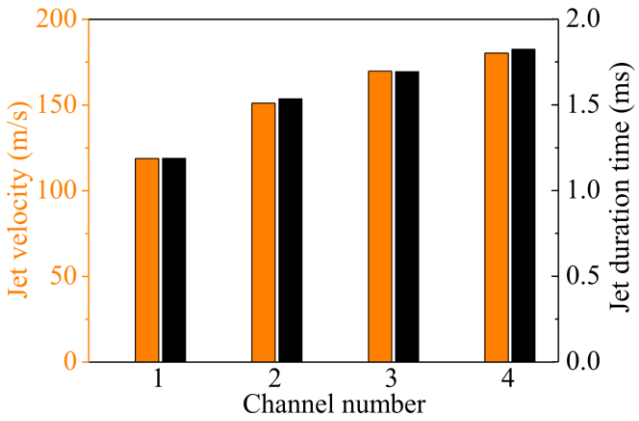

Figure 19. The velocity of the induced jet

The previous research has shown that jet velocity increases with the decrease of chamber volume, while the jet duration time decreases[1,7]. In contrast, with the discharge channel number increase, both the jet velocity and the jet duration time of the ME-PSJA increase. This is because the actuator chamber remains unchanged. Since more discharge channels are used, the discharge efficiency increases, releasing more energy into the actuator chamber. What's more, the heating volume is also enlarged, which benefits the performance of PSJA as well. In all, both the jet velocity and the jet duration time of the ME-PSJA increase with the discharge channel number increase.

4 Conclusions

The present work successfully solves the stringent problems encountered in the use of two-electrode PSJA. A new multichannel discharge circuit is realized through the concept of voltage relay. This circuit allows the increase of total distance of spark channel without using larger input voltage.

The present multi-electrode circuit is able to increase plasma resistance and discharge efficiency, however, the growth flattens out when more electrodes are used. This conclusion is further validated through a five-electrode PSJA. The experiment reveals that the five-electrode PSJA has efficiency two times of that of a two-electrode one. There is also significant increase in jet strength in terms of jet velocity and duration time.

In all, the proposed ME-PSJA opens more application opportunities for the PSJA as it is able to generate stronger jet.

Acknowledgments

This work was sponsored by the National Natural Science Foundation of China (91541120, 51522606, 51336011, 51611130198, 51407197 and 11472306) and Royal Society (IE150612).

References

[1] K. R. Grossman, B. Z. Cybyk and D. M. VanWie, SparkJet Actuators for Flow Control, AIAA 2003-57,2003

[2] Narayanaswamy V, Raja L L, Clemens N T. Control of unsteadiness of a shock wave/turbulent boundary layer interaction by using a pulsed-plasma-jet actuator. Physics of Fluids (1994-present), 2012, 24(7): 076101

[3] Venkat Narayanaswamy, Laxminarayan L. Raja and N.T. Clemens,Control of a Shock/Boundary-layer Interaction by Using a Pulsed-Plasma Jet Actuator,AIAA J,50(2012),246-249,doi:10.2514/1.J051246

[4] T.M. Emerick, M.Y. Ali, C.H. Foster and F.S. Alvi, SparkJet Actuator Characterization in Supersonic Crossflow, 6th AIAA Flow Control Conference, AIAA 2012-2814

[5] Emerick T, Ali M Y, Foster C, et al. SparkJet characterizations in quiescent and supersonic flowfields. Experiments in Fluids, 2014, 55: 1858
[6] Cybyk B Z, Wilkerson J T, Grossman K R. Performance characteristics of the sparkjet flow control actuator, AIAA 2004-2131, 2004
[7] Grossman K R, Cybyk B Z, Rigling M C, et al. Characterization of sparkjet actuators for flow control, AIAA 2004-89, 2004
[8] Cybyk B Z, Grossman K R, Wilkerson J T, et al. Single-pulse performance of the sparkjet flow control actuator, AIAA 2005-401, 2005
[9] Cybyk B Z, Simon D H, Land H, et al. Experimental characterization of a supersonic flow control actuator, AIAA 2006-478, 2006
[10] Cybyk B, Wilkerson J, Simon D. Enabling high-fidelity modeling of a high-speed flow control actuator array, AIAA 2006-8034, 2006
[11] Haack S J, Land H B, Cybyk B, et al. Characterization of a high-speed flow control actuator using digital speckle tomography and PIV, AIAA 2008-3759, 2008
[12] Taylor T M, Cybyk B Z. High-fidelity modeling of micro-scale flow-control devices with applications to the macro-scale environment, AIAA 2008-2608, 2008
[13] Ko H S, Haack S J, Land H B, et al. Analysis of flow distribution from high-speed flow actuator using particle image velocimetry and digital speckle tomography. Flow Measurement and Instrumentation, 2010, 21(4): 443-453
[14] Narayanaswamy V, Raja L L, Clemens N T. Characterization of a high-frequency pulsed-plasma jet actuator for supersonic flow control. AIAA journal, 2010, 48(2): 297-305
[15] Haack S J, Taylor T, Emhoff J, et al. Development of an analytical SparkJet model, 5th Flow Control Conference, AIAA 2010-4979,2010
[16] Haack S J, Taylor T M, Cybyk B Z, et al. Experimental estimation of SparkJet efficiency, AIAA 2011-3997,2011
[17] Golbabaei-Asl M, Knight D, Wilkinson S. Novel technique to determine sparkjet efficiency. AIAA Journal, 2014, 53(2): 501-504
[18] Narayanaswamy V, Raja L L, Clemens N T. Characterization of a high-frequency pulsed-plasma jet actuator for supersonic flow control. AIAA journal, 2010, 48(2): 297-305
[19] Zong H, Wu Y, Song H, et al. Efficiency Characteristic of Plasma Synthetic Jet Actuator Driven by Pulsed Direct-Current Discharge. AIAA Journal, 2016: 3409-3420
[20] Zong H, Wu Y,Jia M,et al. Influence of geometrical parameters on performance of plasma synthetic jet actuator,J. Phys. D: Appl. Phys. 49 (2016) Zong H, Wu Y, Jia M, et al. Influence of geometrical parameters on performance of plasma synthetic jet actuator. Journal of Physics D: Applied Physics, 2015, 49(2): 025504
[21] Popkin S H, Cybyk B Z, Land III H B, et al. Recent performance-based advances in SparkJet actuator design for supersonic flow applications,AIAA 2013-0322,2013
[22] Emerick T, Ali M Y, Foster C, et al. SparkJet characterizations in quiescent and supersonic flowfields. Experiments in Fluids, 2014, 55(12): 1-21
[23] Zong H, Cui W, Wu Y, et al. Influence of capacitor energy on performance of a three-electrode plasma synthetic jet actuator. Sensors and Actuators A: Physical, 2015, 222: 114-121
[24] Zhang Z, Wu Y, Jia M, et al. Influence of the discharge location on the performance of a three-electrode plasma synthetic jet actuator. Sensors and Actuators A: Physical, 2015, 235:

71-79
[25] Reedy T M, Kale N V, Dutton J C, et al. Experimental characterization of a pulsed plasma jet. AIAA journal, 2013, 51(8): 2027-2031
[26] Wang L, Xia Z, Luo Z, et al. Three-electrode plasma synthetic jet actuator for high-speed flow control. AIAA Journal, 2013, 52(4): 879-882
[27] Han M,Zhou X B,Zhang G X.Pulsed Power Technology,Tsinghua University Press,2010
[28] Belinger A, Naudé N, Cambronne J P, et al. Plasma synthetic jet actuator: electrical and optical analysis of the discharge. Journal of Physics D: Applied Physics, 2014, 47(34): 345202
[29] Montanomontano R, Becerra M, Cooray V, et al. Resistance of spark channels. IEEE Transactions on Plasma science, 2006, 34(5): 1610-1619